Towards Modelling AR Sco: Particle Dynamics, Calibration, and First Results

Christo Venter[1]

L du Plessis[1], AK Harding[2], Z Wadiasingh[3,4,5], C Kalapotharakos[4]

[1]Centre for Space Research, North-West University, South Africa
[2]Theoretical Division, Los Alamos National Laboratory
[3]Department of Astronomy, University of Maryland
[4]Astrophysics Science Division, NASA Goddard Space Flight Center
[5]Center for Research and Exploration in Space Science and Technology, NASA/GSFC

NORTH-WEST UNIVERSITY
NOORDWES-UNIVERSITEIT
UNIBESITI YA BOKONE-BOPHIRIMA

Feeling the pull and the pulse of relativistic magnetospheres, 6 – 11 April 2025, Les Houches

AR Sco Observations

- Marsh et al. (2016) detected optical and radio pulsations from the binary white dwarf (WD) system AR Scorpii
- Orbital period 3.55 hours and a "pulsar" spin period of 1.95 min (120 pc).
- Constrained the mass of the WD to $\sim 0.8 M_\odot$ and the M-dwarf companion to $\sim 0.3 M_\odot$
- Stiller et al. (2018) obtained a $\dot{P} = 7.18 \times 10^{-13}\ ss^{-1}$

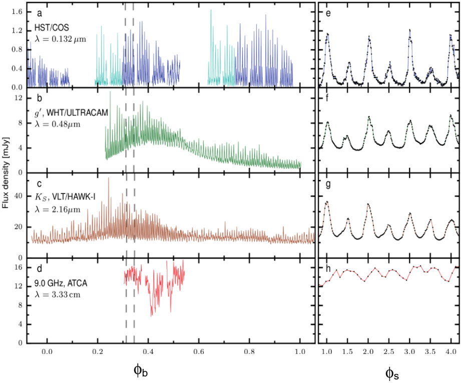

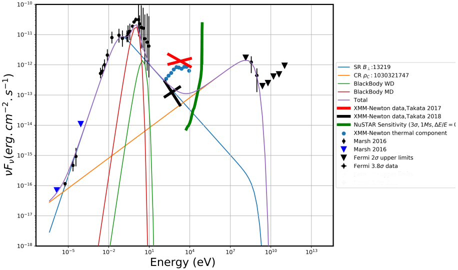

AR Sco Observations

- Optical and UV emission lines show no indication of an accretion disc
- The optical and UV are non-thermal emission and pulsed at the WD spin period
- This gives a light cylinder radius of $R_{\rm LC} = 5.6 \times 10^{11}$ cm and an orbital semi-major axis of $a = 8.5 \times 10^{10}$ cm
- Buckley et al. (2017) found that the system exhibits strong linear optical polarisation (up to $\sim 40\%$) and estimated the WD B-field to be $\sim 500\mathrm{MG}$

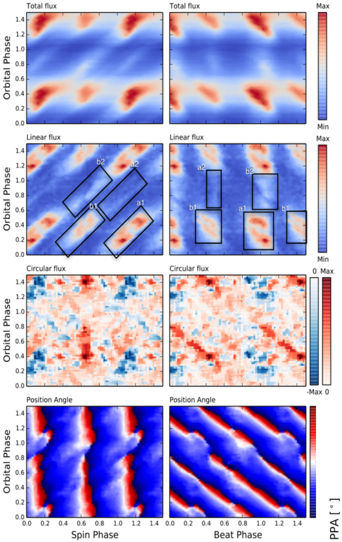

Optical data:
Potter and Buckley (2018)

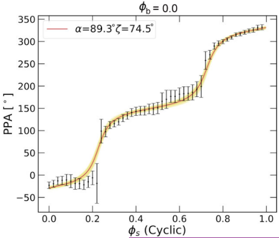

RVM fit: Du Plessis et al. (2019, 2022)
Variation in α and ζ with P_b

Aims

Develop a new general emission model for a WD binary scenario:

- Solve particle dynamics using the general equations of motion.
- Calculate the broadband light curves and spectra at different orbital phases.
- (Calculate Stokes parameters, PPA, and degree of polarisation at different orbital phases.)
- Calibrate our code with the pulsar emission code of Harding and collaborators.

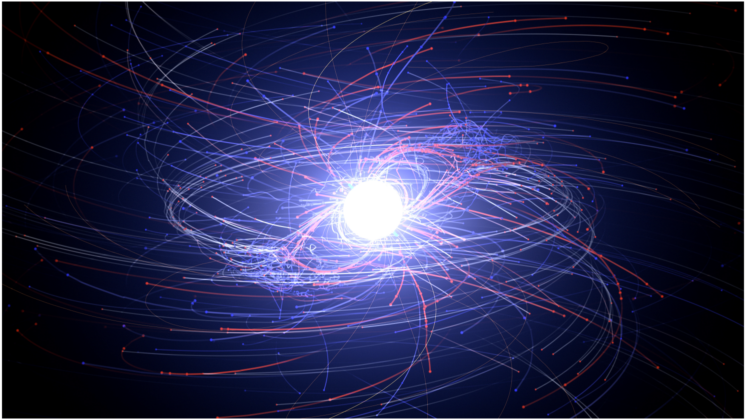

Adaptive ODE Solver

- Solve relativistic Lorentz equation:

$$\frac{d\mathbf{p}}{dt} = q\left(\mathbf{E} + \frac{c\mathbf{p}\times\mathbf{B}}{\sqrt{m^2c^4+\mathbf{p}^2c^2}}\right). \qquad \gamma = \frac{\sqrt{m^2c^4+\mathbf{p}^2c^2}}{mc^2}$$

- Do n-stage evaluations to solve the ODE depending on method accuracy.
- One can calculate the next value by weighing stages, $y_{n+1} = y_n + h\sum_{i=1}^{s} b_i k_i$.
- One can use a method with embedded lower order to get a truncation error, $\tau_{n+1} = y_{n+1} - y^*_{n+1} = \sum_{i=1}^{s}(b_i - b_i^*)k_i$.
- Calculate the adaptive next step size using τ_{n+1} and a given accuracy threshold.

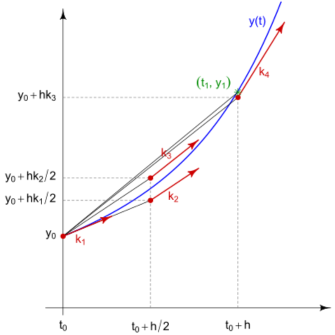

$$\begin{aligned}
k_1 &= f(t_n, y_n),\\
k_2 &= f(t_n + c_2h, y_n + h(a_{21}k_1)),\\
k_3 &= f(t_n + c_3h, y_n + h(a_{31}k_1 + a_{32}k_2)),\\
&\ \ \vdots\\
k_s &= f(t_n + c_sh, y_n + h(a_{s1}k_1 + a_{s2}k_2 + \cdots + a_{s,s-1}k_{s-1})).
\end{aligned}$$

$$\begin{array}{c|cccc}
c_1 & a_{11} & a_{12} & \dots & a_{1s}\\
c_2 & a_{21} & a_{22} & \dots & a_{2s}\\
\vdots & \vdots & \vdots & \ddots & \vdots\\
c_s & a_{s1} & a_{s2} & \dots & a_{ss}\\
\hline
 & b_1 & b_2 & \dots & b_s\\
 & b_1^* & b_2^* & \dots & b_s^*
\end{array}
=
\begin{array}{c|c}
\mathbf{c} & A\\
\hline
 & \mathbf{b^T}
\end{array}$$

Adaptive time step

- Discovered numerical instability from adaptive time step.
- We investigated new higher-precision adaptive-time-step methods.

$$\Delta t_{n+1} = \Delta t_n \left(\frac{TOL}{T_{\mathrm{err}}}\right)^{-\frac{1}{kp}} \left(\frac{TOL}{T_{\mathrm{err;n-1}}}\right)^{-\frac{1}{kp}} \left(\frac{\Delta t_n}{\Delta t_{n-1}}\right)^{-\frac{1}{kp}}. \quad (2)$$

- Δt is the time step, TOL is the chosen tolerance for the truncation error T_{err}, p is the order of the chosen numerical method, and $k = 8$.
- We used a limiting function to constrict the new time step.

$$\Delta t_l = \Delta t_n \left[1 + \kappa arctan\left(\frac{\Delta t_{n+1} - \Delta t_n}{\kappa \Delta t_n}\right)\right]. \quad (3)$$

- $\kappa \in [0.7, 2.0]$.

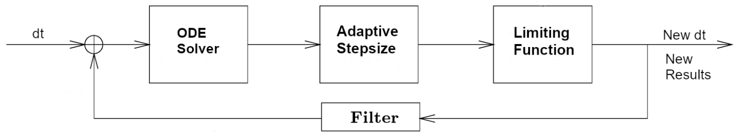

Adaptive ODE Solver

- See **Du Plessis et al. (2024)** for calibration cases and scheme comparisons.
  - Runge-Kutta Fehlberg 4(5): 5 stage.
  - DVERK 6(5): 8 stage.
  - Prince-Dormand 8(7): 12 stage.
  - Adaptive Curtis 10(8): 18 stage.
  - Adaptive Hiroshi 12(9): 29 stage.
  - Vay Symplectic Scheme.

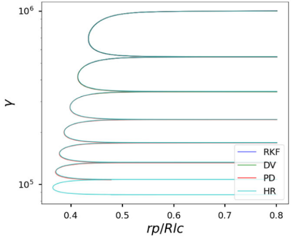

PD: Accurate for larger dt, complete more mirrors

a)

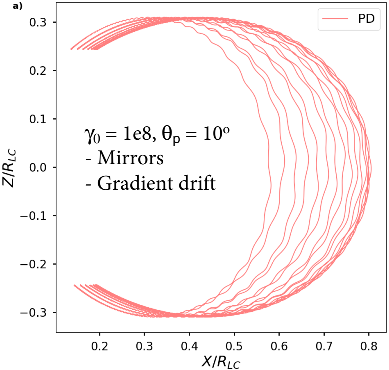

b)

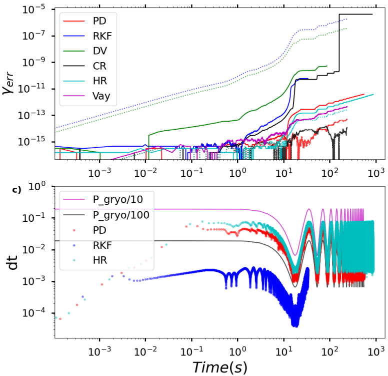

Radiation-Reaction Force

- Use equation from Landau and Lifshitz for general radiation-reaction force:

$$
\begin{aligned}
\mathbf{f} =& \frac{2e^3\gamma}{3mc^3}\left\{\left(\frac{\partial}{\partial t} + \mathbf{v}\cdot\nabla\right)\mathbf{E} + \frac{1}{c}\mathbf{v}\times\left(\frac{\partial}{\partial t} + \mathbf{v}\cdot\nabla\right)\mathbf{H}\right\} \\
&+ \frac{2e^4}{3m^2c^4}\left\{\mathbf{E}\times\mathbf{H} + \frac{1}{c}\mathbf{H}\times(\mathbf{H}\times\mathbf{v}) + \frac{1}{c}\mathbf{E}\left(\mathbf{v}\cdot\mathbf{E}\right)\right\} \\
&- \frac{2e^4\gamma^2}{3m^2c^5}\mathbf{v}\left\{\left(\mathbf{E} + \frac{1}{c}\mathbf{v}\times\mathbf{H}\right)^2 - \frac{1}{c^2}\left(\mathbf{E}\cdot\mathbf{v}\right)^2\right\}.
\end{aligned} \tag{4}
$$

- The first term of Equation 4 requires 9, 18 or 36 evaluations of the B-field per stage to find the derivatives.
- This first term is $\sim 10^8 - 10^{10}$ times smaller than the largest component.
- The super-relativistic form of Equation 4 is given by:

$$
f_x = -\frac{2e^4\gamma^2}{3m^2c^4}\left\{(E_y - H_z)^2 + \left(E_z + H_y^2\right)\right\} \tag{5}
$$

- Equation 4 and 5 converge at a Lorentz factor around $10^4 - 10^5$.

$$
\begin{aligned}
P_{rad} =& \mathbf{F}_{rad}\cdot\mathbf{v}, \\
E_{rad} =& \int \mathbf{F}_{rad}\cdot\mathbf{v}.dt
\end{aligned} \tag{6}
$$

AE Results

- Aristotelian Electrodynamics velocity (gyro-centric):

$$\frac{\mathbf{v}_{AE}}{c} = \frac{\mathbf{E}\times\mathbf{B} \pm (B_0\mathbf{B} + E_0\mathbf{E})}{B^2 + E_0^2}. \quad (7)$$

- $\mathbf{E}\cdot\mathbf{B} = E_0 B_0$, $E^2 + B^2 = E_0^2 + B_0^2$.
- $F_{RRF} > F_L$ in observer frame but not particle frame.

$$\gamma_c = \left(\frac{3E_0 R_c^2}{2|e|}\right)^{\frac{1}{4}}. \quad (8)$$

- θ_D is the angle between $\mathbf{v}$ and $\mathbf{v_{AE}}$.
- Convergence for the radiation-reaction-limited regime.
- $\theta_D \neq 0$ due to gyro-radius.

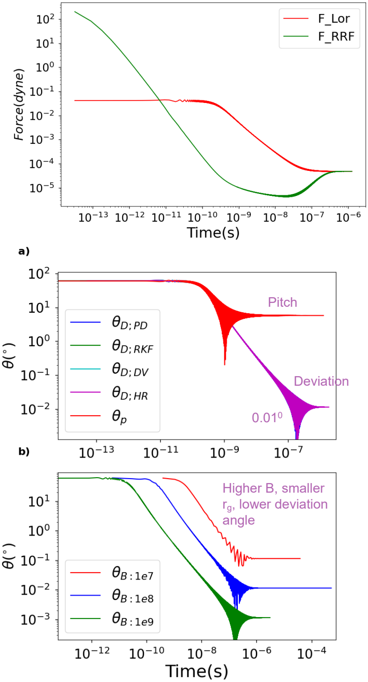

Harding and Collaborators' Code

- Tracing out the particle trajectory incorporating $\mathbf{E} \times \mathbf{B}$ drift from Kalapotharakos et al. (2014).
- $\mathbf{v}/c = \mathbf{E} \times \mathbf{B}/(B^2 + E_0^2) + f\mathbf{B}/B$.
- Solving transport equations from Harding et al. (2005) to calculate emission.
- $d\gamma/dt = eE_{\|}/mc - 2e^4B^2p_{\perp}^2/3m^3c^5$,
- $dp_{\perp}/dt = -3cp_{\perp}/2r - 2e^4B^2p_{\perp}^3/3m^3c^5\gamma$.
- Use CRR-limited γ to stay in classical RRF regime.
- Gyrocentric approach with average particle pitch angle.

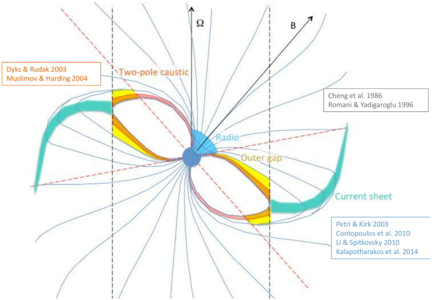

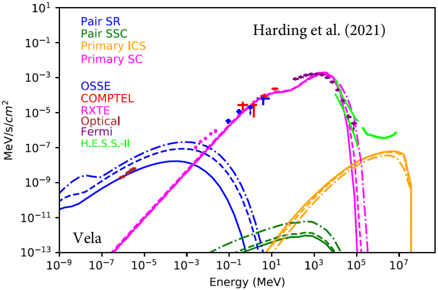

Emission Map Calculations

- We calibrate with vacuum retarded-dipole and force-free fields.
- The phase corrections are given by:
- $\phi_{obs} = \phi_{em} - \mathbf{r}_{\mathbf{em}} \cdot \eta_{\mathbf{em}} / \mathbf{R}_{\mathbf{LC}} - \boldsymbol{\Delta}\phi_{\mathbf{rot}}$
- We use the same curvature- and synchrotron radiation calculations.
- Use $E_{\|}$-component to accelerate particle.

$$R_c = \frac{1}{\sqrt{(x'')^2 + (y'')^2 + (z'')^2}}. \quad (9)$$

- Figures from Barnard et al. (2022) for curvature radiation.

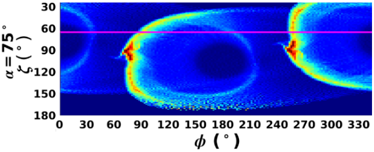

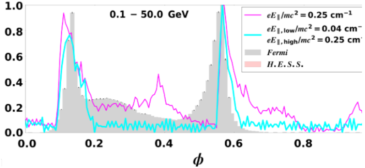

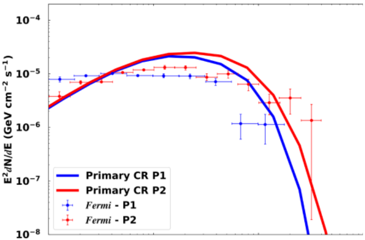

Force-Free Fields

- B- and E-fields have 3 segments for the field structures:
- Vacuum-retarded dipole $R <= 0.2R_{LC}$.
- Force-free fields $0.4R_{LC} <= 2R_{\mathrm{LC}}$.
- Linear combination $0.2R_{LC} < R < 0.4R_{LC}$.
- FF grids generated by Kalapotharakos et al. (2014) model.

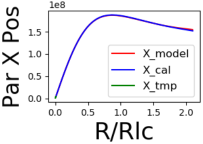

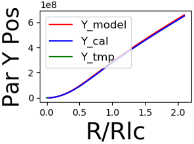

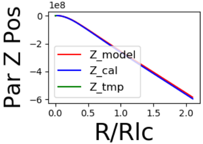

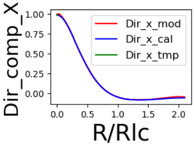

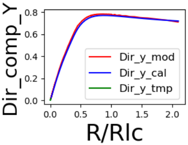

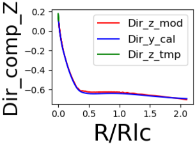

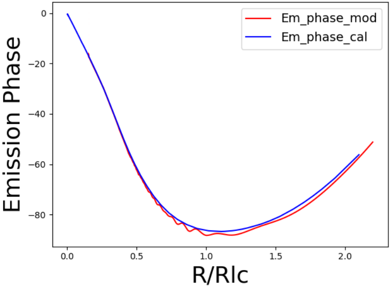

Emission Map Calculations: Skymaps & Spectra

- We first compare curvature radiation.
- We import their radius of curvature.
- Using large fields gives problems at the joining section of the 2 field structures.
- Limit γ with γ_{CRR}.
- We had to use a larger $E_{||}$ inside LC.

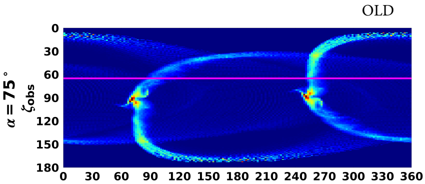

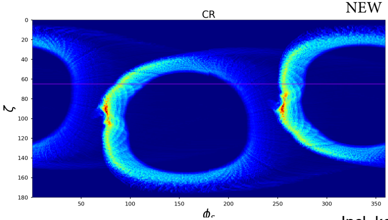

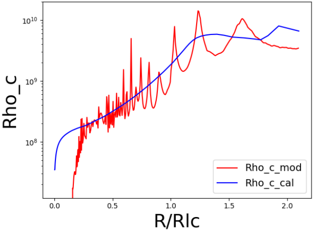

Incl. keV

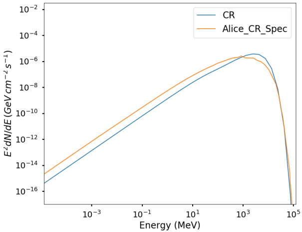

Synchro-curvature Radiation

- Kelner et al. (2015), Cerutti et al. (2016).

$$F_\nu(\nu) = \frac{\sqrt{3}e^3\tilde{B}_\perp}{mc^2}\left(\frac{\nu}{\nu_c}\right)F(y) \quad (10)$$

- $\tilde{B}_\perp = \sqrt{(\mathbf{E} + \beta \times \mathbf{B})^2 + (\beta \cdot \mathbf{E})^2}$.
  - $\rho_{c;eff} = \gamma mc^2 / e\tilde{B}_\perp$
  - Vigano et al. (2015) synchro-curvature (Harding et al. 2021).
  - No E-field and standard θ_p.

$$F_\nu(\nu) = \frac{\sqrt{3}e^2\gamma y}{4\pi\hbar\rho_{eff}} \left[(1+z)F(y) - (1-z)K_{2/3}(y)\right]. \quad (11)$$

$$\rho_{c;eff} = \frac{\rho_c}{\cos^2\theta_p}\left(1 + \zeta + \frac{r_{gyr}}{\rho_c}\right)^{-1} \quad (12)$$

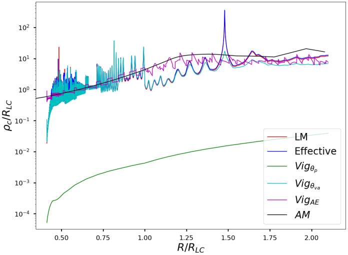

- In the SR regime $\tilde{B}_\perp$ equates to the invariant magnetic field strength perpendicular to the particle motion, instead of just $B_\perp$.
- In CR regime this relates to the radius of curvature.

Emission Maps

a)
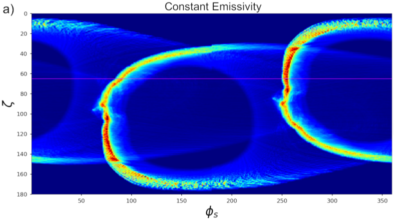

b)
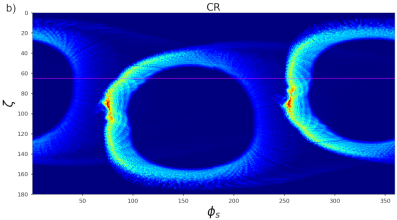

c)
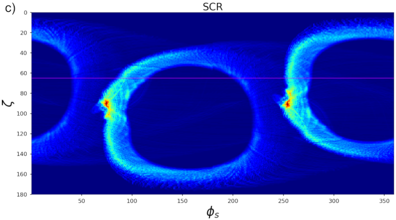

Spectra

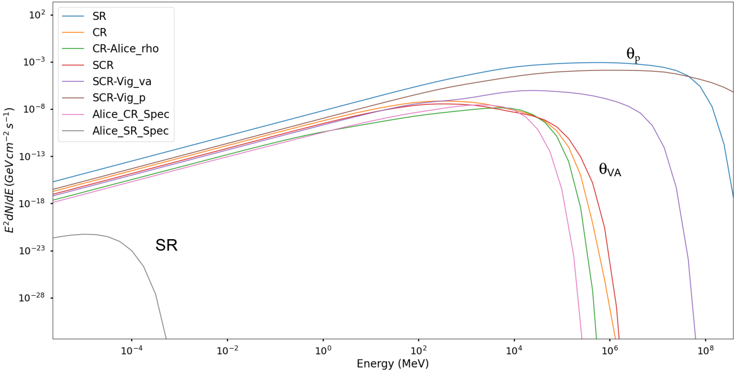

SR
CR
CR-Alice_rho
SCR
SCR-Vig_va
SCR-Vig_p
Alice_CR_Spec
Alice_SR_Spec
θ_p
θ_{VA}
SR
$E^2dN/dE\,(GeV\,cm^{-2}\,s^{-1})$
Energy (MeV)

Outstanding Issues

- The Harding model approach is verified to hold in the limit of a small θ_{VA}.
- There are still outstanding problems to investigate in the Harding model.
- Their transport equations were not robustly re-derived to follow the particle curved trajectory (AE trajectory), with the $\mathbf{E} \times \mathbf{B}$-drift effect neglected in the original derivation.
- The equivalence of using $B \sin\theta$ ($\sin\theta = p/p_\perp$) vs $\tilde{B}_\perp$ in the SR regime.
- Their model only replaces the CR and SR losses with the SCR losses in $d\gamma/dt$ of the transport equations and not in the equation for $dp_\perp/dt$.
- The results should thus be verified in the case were θ_{VA} is not small, i.e in the case were they use resonant photon absorption to boost the 'general pitch angle' for higher SR contributions.

See **Du Plessis et al. (2025, submitted)** for more details.

Initial Comparison with Takata et al. (2019)

- Takata uses rewritten forms of equations from Harding et al. (2005):

$$\frac{d\gamma}{dt} = -\frac{P_\perp^2}{t_s}$$

$$\frac{d}{dt}\left(\frac{P_\perp^2}{B}\right) = -2\frac{B}{t_s\gamma}\left(\frac{P_\perp^2}{B}\right)^2 \quad (13)$$

- where $t_s = 3m_e^3 \quad c^5/2e^4B^2$.
- $P_\perp = \gamma\beta\sin\theta_p$.
- Using a static vacuum dipole our results agree reasonably well.
- Including an $E_\perp$-field there are many more mirrors.

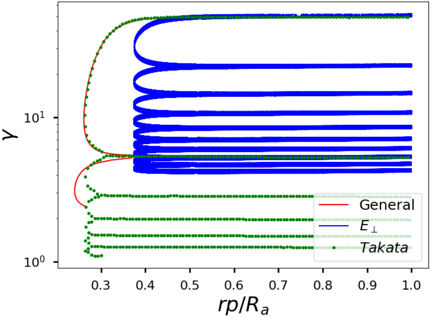

$$\mathbf{E}_\perp = -\frac{\Omega \times \mathbf{r}}{c} \times \mathbf{B}$$

AR Sco Results

- Particles are injected into the WD magnetosphere at the companion.
- The particles are magnetically mirrored close to the WD surface where they are turned around.
- Particles given a standard power-law energy distribution $f(\gamma) = K_0\gamma^{-p}$.
- A uniform θ_p distribution is used to reproduce Takata et al. (2017).
- We only follow 1 field line.
- The WD $E_{\|}$-field is screened.
- We probed different WD B-field strengths, α-values, p-values and including and excluding the $E_{\perp}$-field.

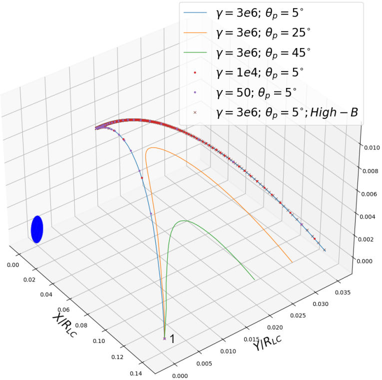

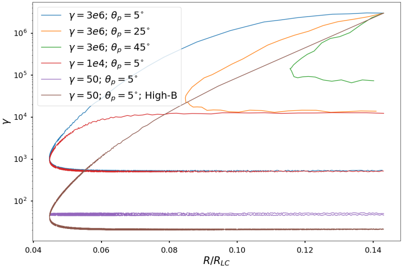

Spectra

- The Takata models use $\zeta = 60°$, $\alpha = 60°$, $B_S \sim 4 \times 10^8$ G, $\gamma_{min} = 50$, $\gamma_{max} = 3 \times 10^6$, excluding $E_\perp$, and use $p = 2.5$ for their 2017 results and $p = 3.0$ for their 2019 results.
- For all our spectra we included $E_\perp$ except the specified case.

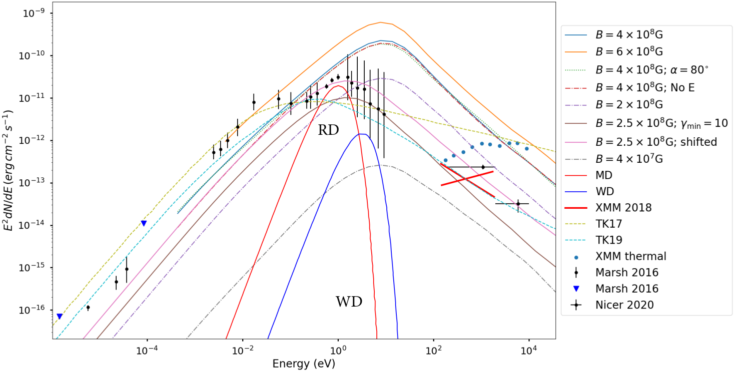

Emission Maps

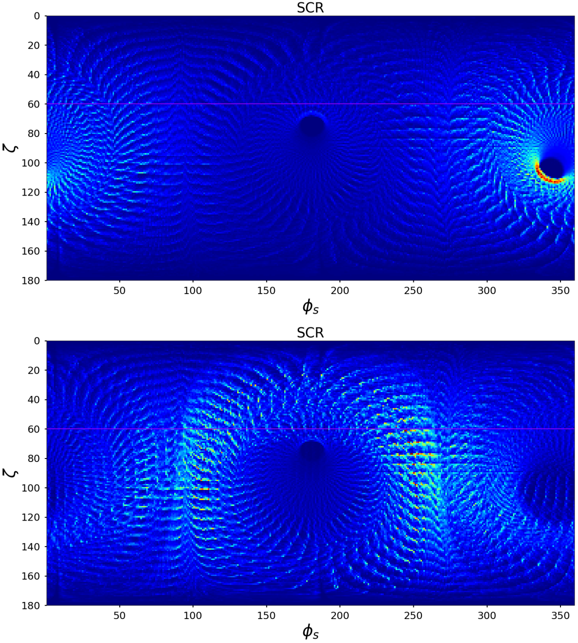

Smaller B
Dominant emission low r

Spectrum not too sensitive on B-field

Higher B
Dominant emission at higher r

Future Work

- Submitted Calibration Paper.
- Finalise results for AR Sco results paper.

Pulsars:

- Calculate fields self consistently to make code full PIC.
- Implement RRF for QED regime to test high-field radiation-reaction limit close to the stellar surface in pulsars.
- Improve computational cost of code: better adaptive time step method, SIMD operations, GPU processing.

AR Sco and similar sources:

- Additional AR Sco modelling: Time-dependent particle injection, build up orbital phase-resolved emission maps, and probe different injection scenarios.
- Implement polarisation calculations to calculate Stokes parameters.
- Model other sources similar to AR Sco or that require general particle dynamics, namely pulsars or intermediate polars.

Bibliography

Buckley, D. A. H., Meintjes, P. J., Potter, S. B., Marsh, T. R., and Gänsicke, B. T. (2017). Polarimetric evidence of a white dwarf pulsar in the binary system AR Scorpii. *Nature Astronomy*, 1:0029.

Marsh, T. R., Gänsicke, B. T., Hümmerich, S., Hambsch, F.-J., Bernhard, K., Lloyd, C., Breedt, E., Stanway, E. R., Steeghs, D. T., Parsons, S. G., Toloza, O., Schreiber, M. R., Jonker, P. G., van Roestel, J., Kupfer, T., Pala, A. F., Dhillon, V. S., Hardy, L. K., Littlefair, S. P., Aungwerojwit, A., Arjyotha, S., Koester, D., Bochinski, J. J., Haswell, C. A., Frank, P., and Wheatley, P. J. (2016). A radio-pulsing white dwarf binary star. *Nature Astronomy*, 537:374–377.

Potter, S. B. and Buckley, D. A. H. (2018). Time series photopolarimetry and modeling of the white dwarf pulsar in AR Scorpii. *Mon. Not. Roy. Astron. Soc.*

Stiller, R. A., Littlefield, C., Garnavich, P., Wood, C., Hambsch, F.-J., and Myers, G. (2018). High-Time-Resolution Photometry of AR Scorpii: Confirmation of the White Dwarf's Spin-Down. *ArXiv e-prints*.